

Effects of quark-matter symmetry energy on hadron-quark coexistence in neutron-star matter

Xuhao Wu,^{1,2,*} Akira Ohnishi,^{2,†} and Hong Shen^{1,‡}

¹*School of Physics, Nankai University, Tianjin 300071, China*

²*Yukawa Institute for Theoretical Physics, Kyoto University, Kyoto 606-8502, Japan*

We examine the effects of the isovector-vector coupling and hypercharge-vector coupling in quark matter on hadron-quark coexistence in neutron-star matter. The relativistic mean field theory with the TM1 parameter set and an extended TM1 parameter set are used to describe hadronic matter, and the Nambu-Jona-Lasinio model with scalar, isoscalar-vector, isovector-vector and hypercharge-vector couplings is used to describe deconfined quark matter. The hadron-quark phase transition is constructed via the Gibbs conditions for phase equilibrium. The isovector-vector and hypercharge-vector couplings in quark matter enhance the symmetry energy and hypercharge symmetry energy in neutron-star matter, while their effects are found to be suppressed at high densities by the strange quarks. As a result, the hadron-quark mixed phase shrinks with only isovector-vector coupling and moves to higher density with isovector-vector and hypercharge-vector couplings. The maximum mass of neutron-star increases slightly with isovector-vector and hypercharge-vector couplings.

PACS numbers: 21.65.Qr, 26.60.Dd, 26.60.Kp, 64.10.+h

Keywords: hadron-quark phase transition, equation of state, isovector-vector coupling

I. INTRODUCTION

Existence of the first-order phase transition in dense neutron-star matter is of primary interest in nuclear physics and compact star astrophysics. In the inner core region of massive neutron stars, the baryon density may reach $(5 - 10)n_0$ ($n_0 \simeq 0.15 \text{ fm}^{-3}$), and the chiral and deconfinement hadron-quark phase transition may occur [1–3]. At present, the sign problem prevents us from predicting the properties of cold dense matter in the first principles calculations such as the lattice QCD Monte Carlo simulations, then phenomenological approaches as well as experimental and observational data are necessary to explore the inner part of neutron stars.

One of the theoretical approaches to study the phase transition is to apply chiral effective models such as the Nambu-Jona-Lasinio (NJL) model. The first-order phase transition can occur at the baryon chemical potential $\mu_b = (1000 - 1200) \text{ MeV}$ using the chiral effective models. Unfortunately, the order of the transition depends on the parameters, and the equation of state (EOS) of nuclear matter at low densities is not well described by the NJL model. Thus it is more realistic to consider the coexistence of hadronic and quark matter in order to predict the transition density. The QCD phase transition signal during the core collapse supernovae was investigated by using a relativistic mean field (RMF) model for hadronic matter and a bag model for quark matter [4, 5], and the early collapse [4] or the

second shock [5] was found to signal the transition to quark matter. In this case, the transition is necessarily of the first order and the transition density strongly depends on the bag constant. The hadron-quark coexistence is investigated also by using RMF for hadronic matter and the NJL model for quark matter [6–8]. In RMF, the isovector-vector meson (ρ) plays an important role to control the symmetry energy in hadronic matter, and the coupling has been carefully chosen to explain the properties of finite nuclei. By comparison, the isovector-vector coupling in quark matter has been considered less carefully. The isovector-vector coupling constant (G_3) was chosen to be $G_3 = 1.5G_0$ in Refs. [7, 9] and $G_3 = G_0$ in Ref. [10], where G_0 is the isoscalar-vector coupling, while the isovector-vector coupling was ignored in Ref. [6]. This difference comes from the two independent types of the chiral $SU(N_f)$ vector coupling terms, $(\bar{q}\gamma_\mu q)^2$ and $\sum_\alpha [(\bar{q}\gamma_\mu \lambda_\alpha q)^2 + (\bar{q}i\gamma_\mu \gamma_5 \lambda_\alpha q)^2]$ [11]. The second type includes the isovector-vector coupling terms and gives rise to symmetry energy in quark matter, the energy increase from the u and d quark imbalance. Since the symmetry energy in nuclear matter is known to affect the neutron-star properties such as radii, it is expected to be important also in the hadron-quark coexistence.

In this work, we examine the role of the isovector-vector coupling in quark matter on the hadron-quark coexistence in neutron-star matter. For this purpose, we apply RMF for hadronic matter and the three-flavor NJL model for quark matter, and we compare the coexistence density region with and without the isovector-vector coupling term in NJL. A finite isovector-vector coupling in quark matter enhances the symmetry energy in quark matter, which characterizes the increase of the energy per baryon from unbalanced u and d quark densities. In addition to this *isospin* symmetry energy,

*Electronic address: wuhaobird@gmail.com

†Electronic address: ohnishi@yukawa.kyoto-u.ac.jp

‡Electronic address: shennankai@gmail.com

the hypercharge symmetry energy appears with $N_f = 3$ and controls the s quark contribution. We also examine the effects of nuclear matter symmetry energy slope L . We use the TM1 parameter set ($L = 110.8$ MeV) [12] and an extended TM1 parameter set (TM1e) [13], where the symmetry energy at the density of $n_b = 0.11$ fm $^{-3}$ is fixed and the symmetry energy slope is tuned to be $L = 50$ MeV. We find that the quark-matter symmetry energy increases the starting density of the hadron-quark coexistence and enhances the maximum mass of neutron stars. The quark-matter symmetry energy effects on the hadron-quark coexistence are suppressed by the s quarks and are smaller than those of the nuclear matter symmetry energy.

There are two comments in order. First, it should be noted that Pereira *et al.* have already discussed the effects of the isovector-vector coupling of quarks on the hadron-quark coexistence, and have found that the isovector-vector coupling pushes up the starting density of the coexistence for a given value of the isoscalar-vector coupling [8]. One of the differences of the present work and Ref. [8] is in the hadronic matter EOS. For hadronic matter, they adopt the NL3 $\omega\rho$ parameter set which derives stiffer EOS at high density than TM1 and TM1e, then most of the parameter sets predict the $1.4M_\odot$ neutron-star radii larger than the range, 10 km $\lesssim R_{1.4} \lesssim 13.6$ km [14], constrained by the gravitational wave observation from a binary neutron-star merger event [15]. Thus it would be valuable to examine TM1e, which predicts smaller neutron-star radii as shown later in Table II. Second, we do not consider here hyperon admixture in neutron stars. If hyperons Λ , Σ , and Ξ are taken into account in a standard way in RMF, the neutron-star maximum mass is known to become much smaller, and many hyperonic matter EOSs cannot support $2M_\odot$, as shown for example in Ref. [16]. One of the ways to avoid this *hyperon puzzle* is to consider additional repulsion for hyperons at high densities, then the hyperon fractions would be smaller and their effect may not be large. Therefore the role of hyperons should be limited, while we need to introduce additional couplings in hadronic matter.

This article is organized as follows. In Sec. II, we introduce the RMF model and the NJL model with the isovector-vector coupling for hadronic and quark matter, and we briefly describe the Gibbs conditions used as the equilibrium conditions in the hadron-quark mixed phase. In Sec. III, we show the numerical results of the hadron-quark coexistence in neutron-star matter and discuss the impact of the isovector-vector coupling. Section IV is devoted to a summary.

II. HADRONIC MATTER, QUARK MATTER AND HADRON-QUARK COEXISTENCE

A. Hadronic matter

We adopt the RMF theory to describe the hadronic phase, in which baryons interact by exchanging the isoscalar scalar (σ), isoscalar vector (ω), and isovector vector (ρ) mesons. These mesons are treated as classical field under the mean field approximation. For neutron-star matter, we use the Lagrangian given as

$$\begin{aligned} \mathcal{L}_{\text{RMF}} = & \sum_{i=p,n} \bar{\psi}_i \left\{ i\gamma_\mu \partial^\mu - (M + g_\sigma \sigma) \right. \\ & \left. - \gamma_\mu \left[g_\omega \omega^\mu + \frac{g_\rho}{2} \tau_a \rho^{a\mu} \right] \right\} \psi_i \\ & + \frac{1}{2} \partial_\mu \sigma \partial^\mu \sigma - \frac{1}{2} m_\sigma^2 \sigma^2 - \frac{1}{3} g_2 \sigma^3 - \frac{1}{4} g_3 \sigma^4 \\ & - \frac{1}{4} W_{\mu\nu} W^{\mu\nu} + \frac{1}{2} m_\omega^2 \omega_\mu \omega^\mu + \frac{1}{4} c_3 (\omega_\mu \omega^\mu)^2 \\ & - \frac{1}{4} R_{\mu\nu}^a R^{a\mu\nu} + \frac{1}{2} m_\rho^2 \rho_\mu^a \rho^{a\mu} \\ & + \Lambda_v (g_\omega^2 \omega_\mu \omega^\mu) (g_\rho^2 \rho_\mu^a \rho^{a\mu}) \\ & + \sum_{l=e,\mu} \bar{\psi}_l (i\gamma_\mu \partial^\mu - m_l) \psi_l, \end{aligned} \quad (1)$$

which contains the contributions of baryons (n and p) and leptons (e and μ). $W^{\mu\nu}$ and $R^{a\mu\nu}$ are the antisymmetric field tensors for ω^μ and $\rho^{a\mu}$, respectively. The parameters in the Lagrangian are usually determined by fitting nuclear matter saturation properties and ground-state properties of finite nuclei. We use the TM1 parameter set [12] and an extended TM1 parameter set [13], referred to as the TM1e parameter set in later discussions. In TM1e, the symmetry energy slope parameter is tuned to be $L = 50$ MeV at saturation density, as listed in Table I. For the homogeneous matter system, the meson field equations have the following form:

$$m_\sigma^2 \sigma + g_2 \sigma^2 + g_3 \sigma^3 = -g_\sigma (n_p^s + n_n^s), \quad (2)$$

$$m_\omega^2 \omega + c_3 \omega^3 + 2\Lambda_v g_\omega^2 g_\rho^2 \rho^2 \omega = g_\omega (n_p + n_n), \quad (3)$$

$$m_\rho^2 \rho + 2\Lambda_v g_\omega^2 g_\rho^2 \omega^2 \rho = \frac{g_\rho}{2} (n_p - n_n), \quad (4)$$

where n_i^s and n_i represent the scalar and vector densities of the i th baryon ($i = n, p$), respectively. The equations of motion for nucleons give the standard relations between the densities and chemical potentials,

$$\mu_p = \sqrt{(k_F^p)^2 + M^{*2}} + g_\omega \omega + \frac{g_\rho}{2} \rho, \quad (5)$$

$$\mu_n = \sqrt{(k_F^n)^2 + M^{*2}} + g_\omega \omega - \frac{g_\rho}{2} \rho, \quad (6)$$

where $M^* = M + g_\sigma \sigma$ is the effective nucleon mass, and k_F^i is the Fermi momentum of species i , which is related to the number density by $n_i = (k_F^i)^3 / 3\pi^2$. For

neutron-star matter in β equilibrium, the chemical potentials satisfy the relations $\mu_p = \mu_n - \mu_e$ and $\mu_\mu = \mu_e$, where the chemical potentials of leptons are given by $\mu_l = \sqrt{k_F^l{}^2 + m_l^2}$. In neutron-star matter, the total energy density and pressure are given by

$$\begin{aligned} \varepsilon = & \sum_{i=p,n} \frac{1}{\pi^2} \int_0^{k_F^i} \sqrt{k^2 + M^{*2}} k^2 dk \\ & + \frac{1}{2} m_\sigma^2 \sigma^2 + \frac{1}{3} g_2 \sigma^3 + \frac{1}{4} g_3 \sigma^4 + \frac{1}{2} m_\omega^2 \omega^2 + \frac{3}{4} c_3 \omega^4 \\ & + \frac{1}{2} m_\rho^2 \rho^2 + 3\Lambda_v (g_\omega^2 \omega^2) (g_\rho^2 \rho^2) + \varepsilon_l, \end{aligned} \quad (7)$$

$$\begin{aligned} P = & \sum_{i=p,n} \frac{1}{3\pi^2} \int_0^{k_F^i} \frac{1}{\sqrt{k^2 + M^{*2}}} k^4 dk \\ & - \frac{1}{2} m_\sigma^2 \sigma^2 - \frac{1}{3} g_2 \sigma^3 - \frac{1}{4} g_3 \sigma^4 \\ & + \frac{1}{2} m_\omega^2 \omega^2 + \frac{1}{4} c_3 \omega^4 + \frac{1}{2} m_\rho^2 \rho^2 \\ & + \Lambda_v (g_\omega^2 \omega^2) (g_\rho^2 \rho^2) + P_l, \end{aligned} \quad (8)$$

where ε_l and P_l ($l = e, \mu$) are the energy density and the pressure from leptons, respectively.

B. quark matter

We adopt the three flavor NJL model to describe the deconfined quark phase. The Lagrangian is given by

$$\begin{aligned} \mathcal{L}_{\text{NJL}} = & \bar{q} (i\gamma_\mu \partial^\mu - m^0) q + G_S \sum_{a=0}^8 \left[(\bar{q} \lambda_a q)^2 + (\bar{q} i\gamma_5 \lambda_a q)^2 \right] \\ & - K \{ \det [\bar{q} (1 + \gamma_5) q] + \det [\bar{q} (1 - \gamma_5) q] \} + \mathcal{L}_V, \end{aligned} \quad (9)$$

with

$$\mathcal{L}_V = -G_0 (\bar{q} \gamma^\mu q)^2 - G_V \sum_{\alpha=1}^8 \left[(\bar{q} \gamma^\mu \lambda_\alpha q)^2 + (\bar{q} i\gamma^\mu \gamma_5 \lambda_\alpha q)^2 \right], \quad (10)$$

in which q denotes the quark field with three flavors ($N_f = 3$) and three colors ($N_c = 3$). The determinant interaction is included in order to take account of the $U(1)_A$ anomaly. G_S , G_0 , and G_V are the scalar, flavor-singlet-vector, and flavor-octet-vector coupling constants, respectively, and have dimensions of energy⁻². In the mean field approximation, only those terms with diagonal matrix elements in λ_α remain, then \mathcal{L}_V is reduced to

$$\begin{aligned} \mathcal{L}_V = & -G_0 (\bar{q} \gamma^\mu q)^2 - G_3 \left[(\bar{q} \gamma^\mu \lambda_3 q)^2 + (\bar{q} i\gamma^\mu \gamma_5 \lambda_3 q)^2 \right] \\ & - G_8 \left[(\bar{q} \gamma^\mu \lambda_8 q)^2 + (\bar{q} i\gamma^\mu \gamma_5 \lambda_8 q)^2 \right]. \end{aligned} \quad (11)$$

In the flavor SU(3) limit, the isovector-vector coupling (G_3) and hypercharge-vector coupling (G_8) constants should be the same, $G_3 = G_8 = G_V$. In order to discuss the (isospin) symmetry energy and the hypercharge symmetry energy effects separately, we consider the cases with $G_3 \neq G_8$ as well.

In the mean field approximation, quarks get constituent quark masses by spontaneous chiral symmetry breaking,

$$m_i^* = m_i^0 - 4G_S \langle \bar{q}_i q_i \rangle + 2K \langle \bar{q}_j q_j \rangle \langle \bar{q}_k q_k \rangle, \quad (12)$$

where $\langle \bar{q}_i q_i \rangle \equiv C_i$ denotes the quark scalar density, and (i, j, k) is a permutation of (u, d, s) . For charge neutral quark matter containing quarks (u, d, s) and leptons (e and μ) in β equilibrium, the chemical potentials satisfy the relations $\mu_s = \mu_d = \mu_u + \mu_e$ and $\mu_\mu = \mu_e$, where the chemical potentials of u, d, s quarks are given by

$$\begin{aligned} \mu_u = & \frac{\partial \varepsilon}{\partial n_u} = \sqrt{k_F^u{}^2 + m_u^{*2}} + 2G_0 (n_u + n_d + n_s) \\ & + 2G_3 (n_u - n_d) + \frac{2}{3} G_8 (n_u + n_d - 2n_s), \end{aligned} \quad (13)$$

$$\begin{aligned} \mu_d = & \frac{\partial \varepsilon}{\partial n_d} = \sqrt{k_F^d{}^2 + m_d^{*2}} + 2G_0 (n_u + n_d + n_s) \\ & - 2G_3 (n_u - n_d) + \frac{2}{3} G_8 (n_u + n_d - 2n_s), \end{aligned} \quad (14)$$

$$\begin{aligned} \mu_s = & \frac{\partial \varepsilon}{\partial n_s} = \sqrt{k_F^s{}^2 + m_s^{*2}} + 2G_0 (n_u + n_d + n_s) \\ & - \frac{4}{3} G_8 (n_u + n_d - 2n_s). \end{aligned} \quad (15)$$

The energy density of quark matter is given by

$$\begin{aligned} \varepsilon_{\text{NJL}} = & \sum_{i=u,d,s} \left[-\frac{3}{\pi^2} \int_{k_F^i}^\Lambda \sqrt{k^2 + m_i^{*2}} k^2 dk \right] \\ & + 2G_S (C_u^2 + C_d^2 + C_s^2) - 4K C_u C_d C_s \\ & + G_0 (n_u + n_d + n_s)^2 \\ & + G_3 (n_u - n_d)^2 \\ & + \frac{1}{3} G_8 (n_u + n_d - 2n_s)^2 - \varepsilon_0, \end{aligned} \quad (16)$$

where ε_0 is subtracted to ensure $\varepsilon_{\text{NJL}} = 0$ in the vacuum. The total energy density and pressure for quark matter are given by

$$\varepsilon_{\text{QP}} = \varepsilon_{\text{NJL}} + \varepsilon_l, \quad (17)$$

$$P_{\text{QP}} = \sum_{i=u,d,s,e,\mu} n_i \mu_i - \varepsilon_{\text{QP}}. \quad (18)$$

We employ the parameter set given in Ref. [9], $m_u^0 = m_d^0 = 5.5$ MeV, $m_s^0 = 140.7$ MeV, $\Lambda = 602.3$ MeV, $G_S \Lambda^2 = 1.835$, and $K \Lambda^5 = 12.36$. The vector couplings (G_0, G_3, G_8) are considered as free parameters, and we use $G_0 = 0.25 G_S$, $G_3, G_8 = (0, 1.5, 10) G_0$. For larger G_0 values ($G_0 > 0.27 G_S$), the energy in quark matter is found to be always larger than that in hadronic matter

TABLE I: Parameters in the TM1 and TM1e parameter sets. The masses are given in the unit of MeV.

Model	$L(\text{MeV})$	M	m_σ	m_ω	m_ρ	g_σ	g_ω	g_ρ	$g_2 (\text{fm}^{-1})$	g_3	c_3	Λ_v
TM1	110.8	938.0	511.198	783.0	770.0	10.0289	12.6139	9.2644	-7.2325	0.6183	71.3075	0
TM1e	50	938.0	511.198	783.0	770.0	10.0289	12.6139	12.2413	-7.2325	0.6183	71.3075	0.0327

at high densities, and there is no phase transition. The parameter choice of $G_3 = G_8 = 1.5 G_0$ corresponds to the Lagrangian adopted in Refs. [7, 9]. The larger isovector-vector coupling, $G_3 = G_8 = 10 G_0$, roughly gives the symmetry energy slope of $L_Q \simeq 50$ MeV. The vector couplings increase the energy per baryon as

$$\frac{\Delta \varepsilon_V}{n_b} = 9 G_0 n_b + G_3 n_b \delta^2 + 3 G_8 n_b \delta_h^2, \quad (19)$$

$$\delta = \frac{n_d - n_u}{n_b}, \quad \delta_h = \frac{n_b - n_s}{n_b} = \frac{B + S}{B}. \quad (20)$$

There are two types of asymmetry parameter, δ and δ_h , which are the isospin asymmetry and the hypercharge ($Y = B + S$) fraction. The symmetry energy is defined as the coefficient of δ^2 , then the vector coupling contribution to the symmetry energy is given as

$$\Delta S_V(n_b) = G_3 n_b = G_3 n_0 + 3 G_3 n_0 \left(\frac{n_b - n_0}{3n_0} \right). \quad (21)$$

The vector coupling contribution to the slope parameter is $\Delta L_V = 3G_3 n_0 = 6.6$ and 44 MeV for $G_3 = 1.5G_0$ and $10G_0$, respectively.

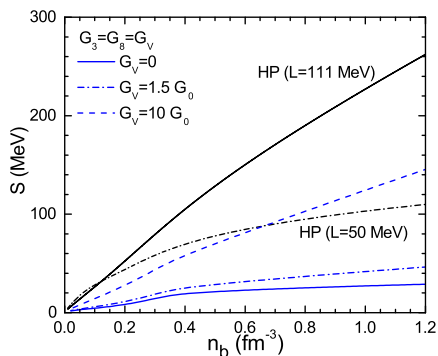


FIG. 1: (Color online) Symmetry energy as a function of the baryon number density for the pure hadronic phase (black lines) and the pure quark phase (blue lines) with different vector couplings.

In Fig. 1, we compare the symmetry energy S as a function of baryon number density n_b for the pure hadronic matter and pure quark matter. The results of $G_3 = G_8 = 0, 1.5G_0$, and $10G_0$ are shown. Usually the quark matter symmetry energy is much smaller than the TM1e with

$G_3 = G_8 = 0$ or $1.5G_0$, while with $G_3 = G_8 = 10G_0$, the result is comparable to TM1e ($L = 50$ MeV). Thus the parameter sets with $G_3 = G_8 = (0 - 10)G_0$ covers a wide and reasonable range of symmetry energy.

C. Hadron-quark phase transition

For neutron-star matter, the β equilibrium and the charge neutrality are satisfied. We adopt simple Gibbs conditions for the mixed phase connecting the pure hadronic phase and the pure quark phase. The mixed phase may appear in the inner core of the neutron stars.

In the Gibbs conditions, the global charge neutrality condition is given by

$$un_c^{\text{QP}} + (1 - u)n_c^{\text{HP}} = 0, \quad (22)$$

in which $u = V_{\text{QP}}/(V_{\text{QP}} + V_{\text{HP}})$ represents the volume fraction of quark matter in the mixed phase. The mechanical equilibrium requires

$$P_{\text{HP}}(\mu_n, \mu_e) = P_{\text{QP}}(\mu_n, \mu_e). \quad (23)$$

There are two independent chemical potentials, μ_n and μ_e ; the hadronic and quark phases satisfy the chemical equilibrium condition,

$$\mu_u + \mu_e = \mu_d = \mu_s = \frac{\mu_n}{3} + \frac{\mu_e}{3}. \quad (24)$$

With these equilibrium constraints, we can solve the mixed phase self-consistently and obtain the properties of the hadron-quark mixed phase.

III. ISOVECTOR-VECTOR COUPLING DEPENDENCE OF HADRON-QUARK COEXISTENCE IN NEUTRON-STAR MATTER

We shall now investigate the effects of isovector-vector coupling on the equation of state, the density range of hadron-quark coexistence, and the properties of neutron stars. For this intent, we use the RMF and NJL models to describe hadronic and quark matter, respectively. For RMF, the TM1 and TM1e parameter sets are used. These parameter sets show different symmetry energy slopes (L), which show significant effects on the neutron-star radius. We include isovector-vector coupling in NJL, which modifies the quark-matter symmetry energy. In

TABLE II: Model dependence of the coexistence densities and neutron-star properties, $G_0 = 0.25G_S$.

Model	L (MeV)	G_3/G_0	G_8/G_0	$n_b^{(1)}$ (fm $^{-3}$)	$n_b^{(2)}$ (fm $^{-3}$)	M_{\max}/M_\odot	$n_c^{M_{\max}}$ (fm $^{-3}$)	$R(1.4 M_\odot)$ (km)
TM1	110.8	-	-	-	-	2.180	0.871	14.3
TM1/NJL-V	110.8	0	0	0.508	2.209	2.098	0.769	14.3
TM1/NJL-VR1	110.8	1.5	0	0.565	2.168	2.125	0.816	14.3
TM1/NJL-VRY1	110.8	1.5	1.5	0.565	2.225	2.125	0.815	14.3
TM1/NJL-VR2	110.8	10	0	0.687	2.067	2.163	0.850	14.3
TM1/NJL-VRY2	110.8	10	10	0.718	2.240	2.170	0.830	14.3
TM1e	50	-	-	-	-	2.122	0.899	13.0
TM1e/NJL-V	50	0	0	0.681	2.210	2.103	0.900	13.0
TM1e/NJL-VR1	50	1.5	0	0.753	2.170	2.114	0.881	13.0
TM1e/NJL-VRY1	50	1.5	1.5	0.757	2.226	2.115	0.879	13.0
TM1e/NJL-VR2	50	10	0	0.890	2.076	2.122	0.888	13.0
TM1e/NJL-VRY2	50	10	10	0.938	2.241	2.122	0.888	13.0
Constraints	40~60 [17]	-	-	-	-	1.928 ± 0.017 [18, 19]	-	12 ± 1 [21]
						2.01 ± 0.04 [20]	-	9.4 ± 1.2 [22]
								> 14 [23]

the following discussions, we fix the isoscalar-vector coupling as $G_0 = 0.25G_S$, and we compare the results of $(G_3/G_0, G_8/G_0) = (0, 0), (1.5, 0), (1.5, 1.5), (10, 0)$, and $(10, 10)$, referred to as NJL-V, NJL-VR1, NJL-VRY1, NJL-VR2, and NJL-VRY2, respectively. NJL-V and NJL-VRY1 corresponds to models in Ref. [6] and Refs. [7, 9], respectively.

We define $n_b^{(1)}$ and $n_b^{(2)}$ as the starting and the ending baryon densities of the mixed phase. At the density $n_b^{(1)}$, the energy per baryon in the mixed phase becomes lower than that of pure hadronic phase. The volume fraction of quark matter u increases with the baryon number density n_b , and it transforms into pure quark phase at the density $n_b^{(2)}$ under the condition that the mixed phase has larger energy density than the pure quark phase. The model dependence of the phase transition densities $n_b^{(1)}$ and $n_b^{(2)}$ is summarized in Table II.

A. Equation of state

We first discuss the equation of state. In Fig. 2, we show the pressure as a function of the baryon number density for hadronic matter, quark matter, and the mixed phase obtained under Gibbs conditions. The top and bottom panels show the results from the TM1 ($L = 110.8$ MeV) and TM1e ($L = 50$ MeV) parameter sets, respectively. The left, middle, and right panels show the results of NJL-V ($G_3 = G_8 = 0$), NJL-VRY1 ($G_3 = G_8 = 1.5G_0$), and NJL-VRY2 ($G_3 = G_8 = 10G_0$), respectively.

In Fig. 3, we compare the energy per baryon, $E/A - M$, as a function of baryon number density n_b for

the hadronic, mixed, and quark phases. Open circles (squares, triangles) show the transition densities of NJL-V (NJL-VRY1, NJL-VRY2). We find isovector-vector and hypercharge-vector couplings delay the transition to the mixed phase. Although the energy difference between NJL-V, NJL-VR1, and NJL-VR2 is small in quark matter, the $n_b^{(1)}$ difference is very visible, whereas the $n_b^{(2)}$ difference is rather small. The reason comes from the difference of the isospin and hypercharge asymmetry of quarks, $\delta_Q = 3(n_d - n_u)/(n_d + n_u + n_s)$ and $\delta_b^Q = (n_u + n_d - 2n_s)/(n_d + n_u + n_s)$, in the pure quark phase and in the mixed phase. In the mixed phase, the quark matter part is negatively charged and the number density difference between u quark and d quark (so as hypercharge difference) is bigger than that in the charge neutral pure quark phase as can be found from the electron chemical potential discussed below.

We show the electron chemical potential as a function of the neutron chemical potential (the baryon density) in the left (right) panel of Fig. 4. The electron chemical potential μ_e in the mixed phase is significantly larger than that in the pure quark matter at the same baryon number density n_b . The electron chemical potential μ_e reflects the chemical potential difference of the u and d quarks ($\mu_d - \mu_u = \mu_e$). It can be seen as a signal of the imbalance between u and d quarks. The system becomes more symmetric with decreasing μ_e . The behavior of μ_e can explain why the effect of isovector-vector coupling is more significant at lower densities. For pure quark matter, there exists a maximum value of μ_e , which corresponds to the appearance of s quark. This change expresses that the imbalance between u and d quarks is getting smaller. These trends are the same as those found

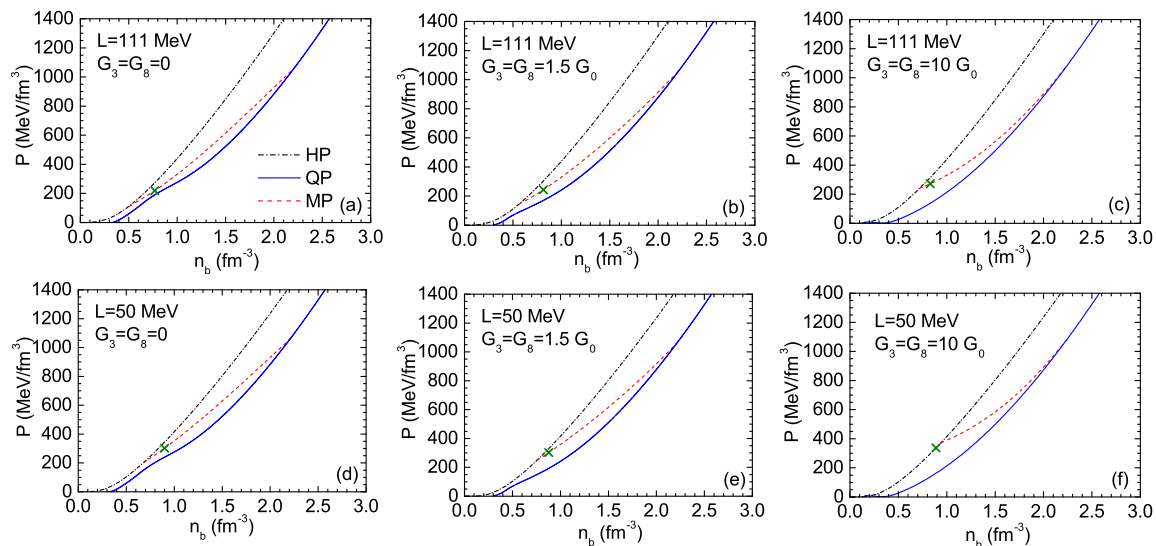


FIG. 2: (Color online) Pressures as a function of the baryon number density for the pure hadronic phase (dash-dotted lines), the mixed phase (dashed lines), and the pure quark phase (solid lines).

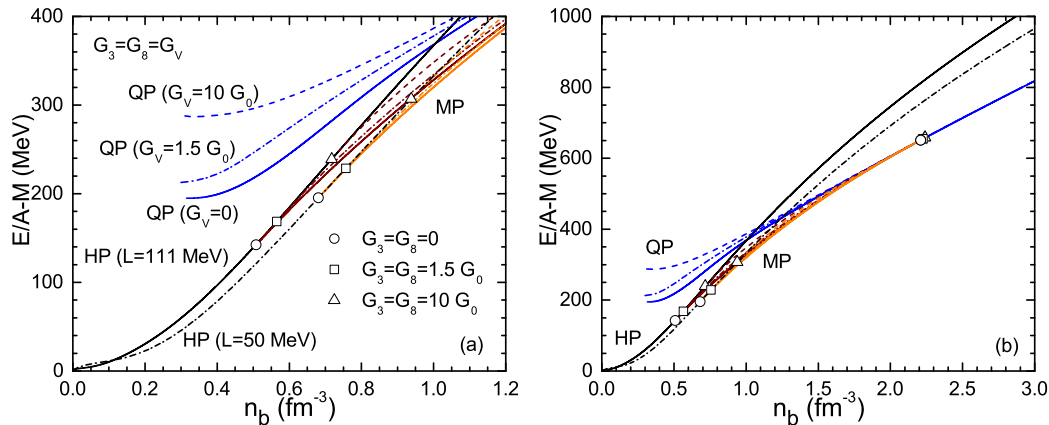


FIG. 3: (Color online) Energy density per baryon as a function of the baryon number density for the hadronic, mixed, and quark phases. The left panel is a local enlargement of the right panel. Open circles (squares, triangles) label the transition points for $G_3 = G_8 = 0$ ($G_3 = G_8 = 1.5G_0$, $G_3 = G_8 = 10G_0$).

in Fig. 3.

It would be interesting to discuss the reason why the electron chemical potential is small in pure quark matter. In Fig. 4, we find that μ_e in pure quark matter increases at low densities, reaches $\mu_e \simeq 100$ MeV, and turns to decrease at around $\mu_n = 1300$ MeV. At this density, the quark chemical potentials are evaluated as $\mu_u \simeq 370$ MeV and $\mu_d = \mu_s \simeq 470$ MeV. Since the chemical potential of s quark is close to its threshold value for appearance, then we expect that the appearance of s quarks would be the mechanism to suppress the electron chemical potential.

We find that the mixed phase shrinks when the

isovector-vector coupling (G_3) and hypercharge-vector coupling (G_8) are switched on. Two couplings, G_3 and G_8 , modify both of the transition densities, and the shift of $n_b^{(1)}$ is larger than that of $n_b^{(2)}$. This difference comes from the density dependence of the isospin asymmetry, $\delta \equiv ((1-u)(n_n - n_p) + u(n_d - n_u))/n_b$. In the hadron-quark mixed phase, the matter tends to be more symmetric with increasing baryon number density n_b . At $n_b \simeq n_b^{(1)} < 0.9 \text{ fm}^{-3}$, the isospin asymmetry δ is still significant, while δ is almost zero at $n_b \simeq n_b^{(2)} > 2.3 \text{ fm}^{-3}$. Since the energy from the isovector-vector coupling is

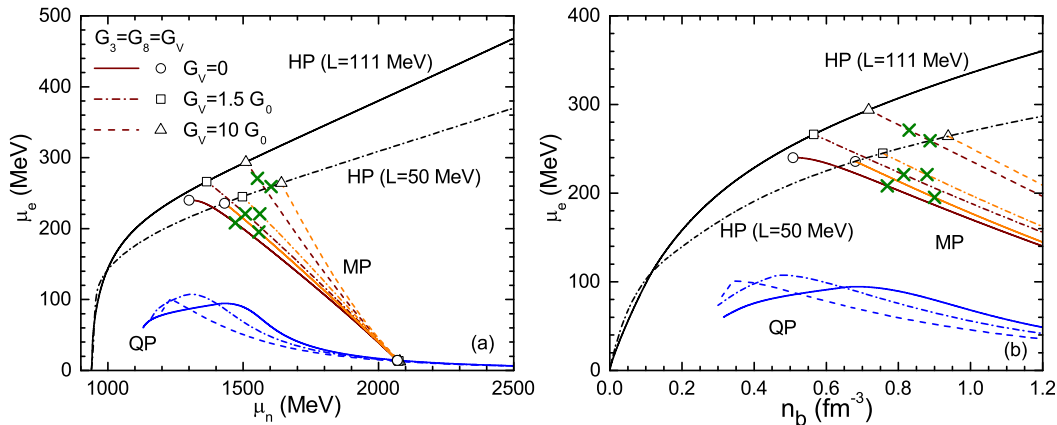


FIG. 4: (Color online) The left panel shows the relation between the chemical potential of neutron and electron. The right panel is the electron chemical potential as a function of baryon number density for different phases.

proportional to δ^2 , it becomes small at high baryon densities. This mechanism also applies to the effect of the symmetry energy slope L .

B. Particle fraction and asymmetry

We now discuss the isovector-vector coupling (G_3) and hypercharge-vector (G_8) coupling effects in terms of the isospin asymmetry (δ) and hypercharge fraction (δ_h). We show δ (δ_h) as a function of the baryon number density in the top (bottom) two rows in Fig. 5. We first find that G_3 and G_8 obviously suppress δ and δ_h in the pure quark phase and the mixed phase. We also note that δ decreases rapidly when the s quark appears and δ_h becomes smaller than unity. With increasing n_b , the effect from different symmetry energy slope L becomes smaller. Finite G_3 and G_8 increase the energy and delay the appearance of the mixed phase, i.e., two couplings push up $n_b^{(1)}$. By comparison, $n_b^{(2)}$ is determined by both the energy increase and the asymmetry decrease in quark matter. The increase of the energy in quark matter pushes up $n_b^{(2)}$. The decrease of δ and thus μ_e tends to make coexisting hadronic matter isospin symmetric and positively charged, disfavors the mixed phase, and pushes down $n_b^{(2)}$. When both G_3 and G_8 are switched on, effects from the energy increase and the asymmetry decrease seem to cancel, and $n_b^{(2)}$ is almost the same as that without G_3 and G_8 . When only G_3 is switched on, effects from the asymmetry decrease are larger than those from the energy increase, then $n_b^{(2)}$ decreases slightly.

Let us further discuss the effects of quark-matter symmetry energy on particle fractions. In Fig. 6, we show the particle number fractions in hadron matter, quark mat-

ter, and the mixed phase, as functions of the baryon number density. As already mentioned, the electron chemical potential in the mixed phase is larger than that in pure quark matter, and therefore the fractions of d and s quarks in the mixed phase are larger than those in quark matter. When the isovector-vector coupling G_3 and hypercharge-vector coupling G_8 are taken into account, the differences between quark fractions become smaller and the quark matter tends to be more SU(3) symmetric. When the s quark appears, the differences between the u quark and d quark are suppressed furthermore.

C. Neutron stars

Using the EOS of pure hadronic matter, the TM1 parameter set predicts a maximum neutron-star mass of $2.18M_\odot$, with M_\odot being the solar mass. The neutron-star observations of PSR J1614-2230 [18, 19] and PSR J0348+0432 [20] constrain that the neutron-star maximum mass needs to be larger than $2M_\odot$. To examine the effect of isovector-vector coupling G_3 and hypercharge-vector coupling G_8 on the properties of neutron stars, we solve the Tolman-Oppenheimer-Volkoff (TOV) equation by using models listed in Table II. The mass-radius relation is presented in the left panel of Fig. 7. The right panel shows the neutron-star mass as a function of the neutron-star central density n_c . We also identified the central density of the maximum mass star in Figs. 2, 4, 5, and 6 by green cross marks, which show clearly where the central density of the maximum mass is located. With models TM1, TM1e/NJL-V, and TM1e/NJL-VRY1, the central density may locate in the mixed phase close to the first transition density $n_b^{(1)}$, while the central den-

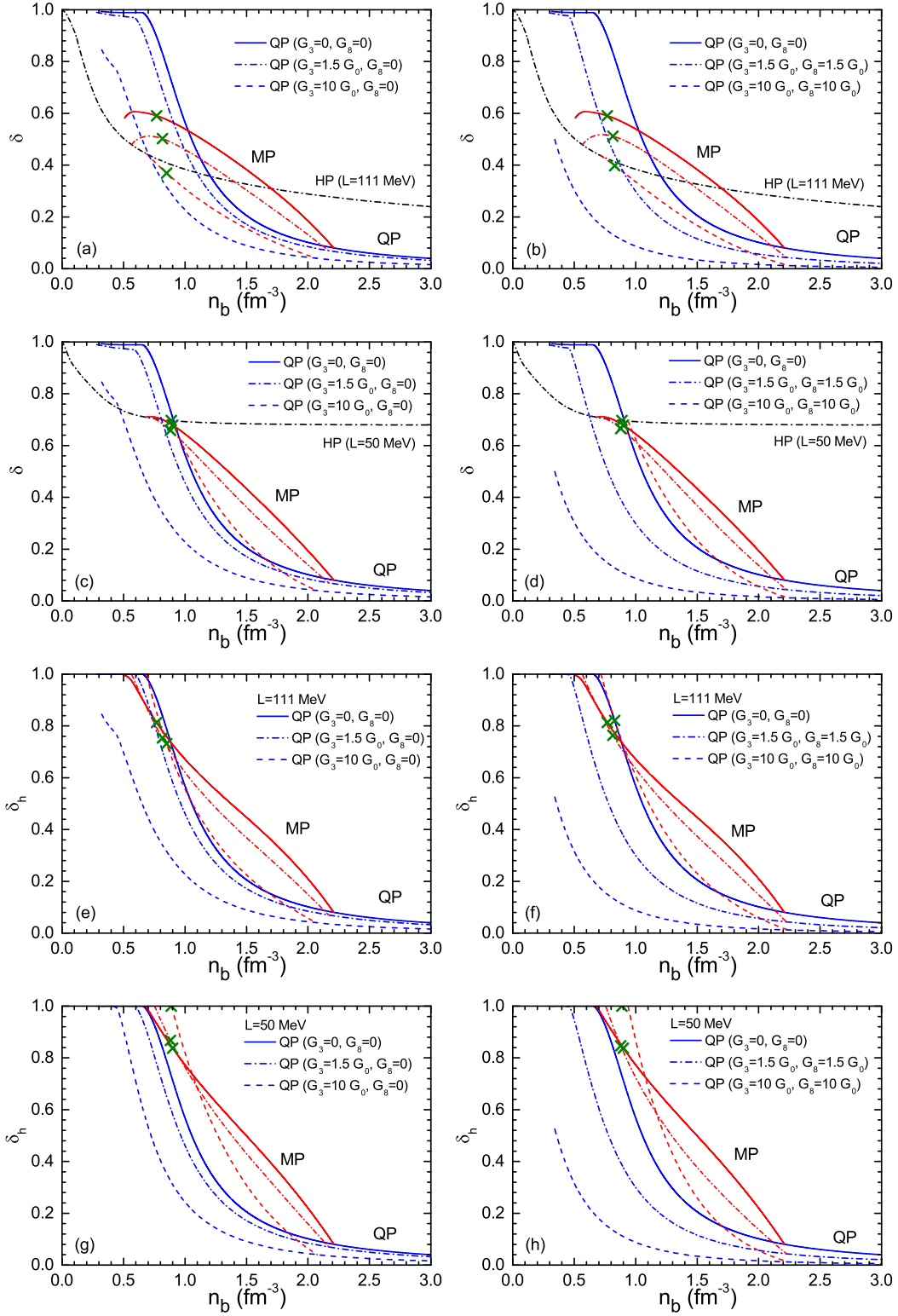


FIG. 5: (Color online) The isospin asymmetry and hypercharge fraction for $(G_3/G_0, G_8/G_0) = (0, 0), (1.5, 0), (1.5, 1.5), (10, 0)$, and $(10, 10)$.

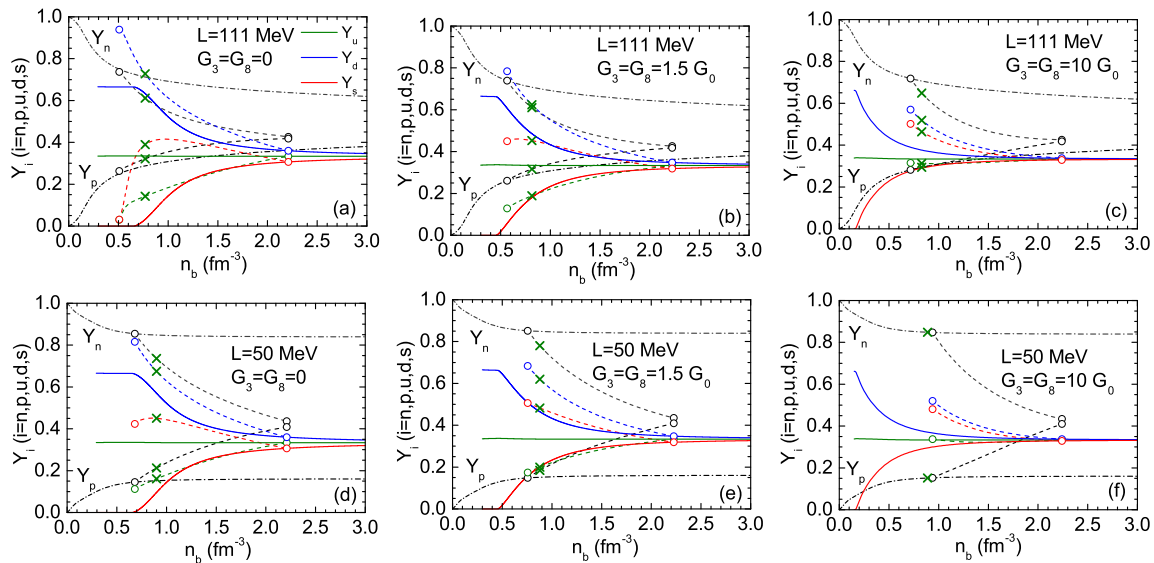


FIG. 6: (Color online) Particle number fractions for the pure hadronic phase (dash-dotted lines), the mixed phase (dashed lines) and the pure quark phase (solid lines). The fractions of u , d , and s quarks are labeled by green (middle), blue (upper), red (lower) solid lines in the pure quark phase and green (lower), blue (upper), red (middle) dashed lines in the mixed phase.

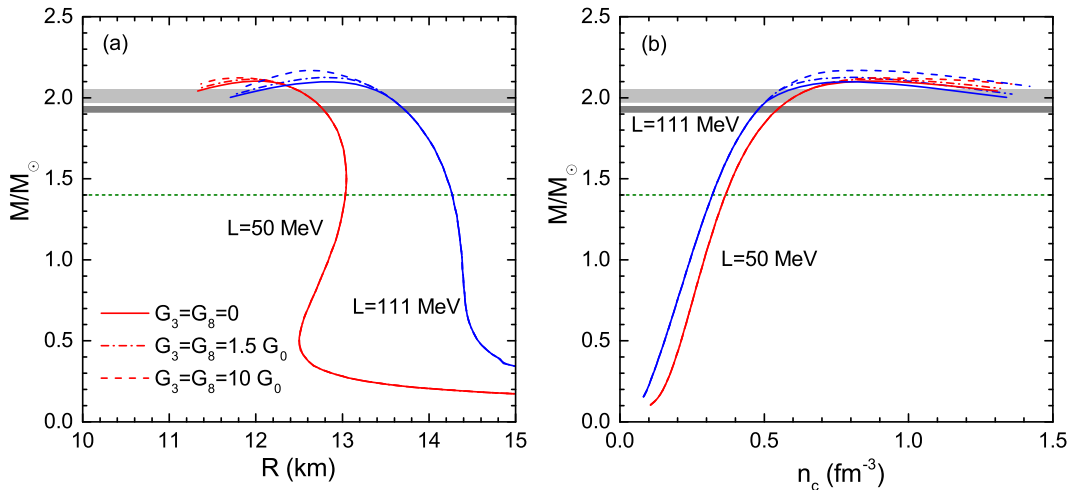


FIG. 7: (Color online) The left panel plots mass-radius relations of neutron stars for different EOS. The solid lines and the dash-dotted lines (dashed lines) show the results without and with isovector-vector coupling and hypercharge-vector coupling respectively. The right panel shows maximum mass as a function of neutron-star central density.

sity locates in the pure hadronic matter with model TM1e/NJL-VRY2. We find that the isovector-vector coupling enhances the maximum mass of neutron stars slightly, but the effect is inconspicuous. For the results of TM1e ($L = 50$ MeV), it shows a smaller radius than that of TM1 ($L = 110.8$ MeV). The influence of G_3 on neutron-star maximum mass becomes even smaller with TM1e. This is because the onset of the mixed phase in TM1e is later than that in TM1. In the right panel of Fig. 7, we can see that when the transition density $n_b^{(1)}$ is

close to the maximum neutron star central density $n_c^{M_{\max}}$ (for TM1e case), the hadron-quark coexistence has little effect for the maximum mass neutron stars.

IV. SUMMARY

Effects of the isovector-vector and hypercharge-vector couplings in quark matter on hadron-quark phase transition and neutron-star properties are investigated. In

this work, we have used the RMF theory to describe hadronic matter, and the three flavor NJL model including the isovector-vector coupling has been used for the quark matter. The Gibbs conditions are applied to describe the hadron-quark mixed phase. We have found that the mixed phase shrinks with the isovector-vector coupling in quark matter, while the mixed phase moves to higher density with both isovector-vector and hypercharge-vector couplings included. If only isovector-vector coupling is included in quark matter, the transition density to the mixed phase ($n_b^{(1)}$) increases by $(0.06 - 0.25) \text{ fm}^{-3}$, and the transition density to the pure quark matter ($n_b^{(2)}$) decreases by $(0.04 - 0.14) \text{ fm}^{-3}$. The hypercharge-vector coupling delays both $n_b^{(1)}$ and $n_b^{(2)}$. The inclusion of the isovector-vector and hypercharge-vector couplings in quark matter has similar effects as decreasing the symmetry energy slope L in hadronic matter. Both of them can affect the asymmetry of the system. We have found that the isovector-vector and hypercharge-vector couplings suppress the asymmetry of

the nuclear-quark matter system. Meanwhile, the softening of the EOS due to the hadron-quark phase transition becomes weaker and the neutron-star maximum mass increases without modifying the neutron-star radius around $M \sim 1.4 M_\odot$, where the central density is $n_b \sim (2 - 3) n_0$.

Acknowledgment

This work was supported in part by the Grants-in-Aid for Scientific Research from JSPS (Grants No. 15K05079, No. 15H03663, and No. 16K05350), the Grants-in-Aid for Scientific Research on Innovative Areas from MEXT (Grants No. 24105001 and No. 24105008), the National Natural Science Foundation of China (Grants No. 11675083), and by the Yukawa International Program for Quark-hadron Sciences (YIPQS). X. W. acknowledges the financial support provided by the China Scholarship Council (CSC).

-
- [1] N. K. Glendenning, Phys. Rep. **342**, 393 (2001).
 [2] H. Heiselberg and M. Hjorth-Jensen, Phys. Rep. **328**, 237 (2000).
 [3] F. Weber, Prog. Part. Nucl. Phys. **54**, 193 (2005).
 [4] K. Nakazato, K. Sumiyoshi, and S. Yamada, Phys. Rev. D **77**, 103006 (2008).
 [5] I. Sagert, M. Hempel, G. Pagliara, J. Schaffner-Bielich, T. Fischer, A. Mezzacappa, F.-K. Thielemann and M. Liebendörfer, Phys. Rev. Lett. **102**, 081101 (2009).
 [6] S. Benic, D. Blaschke, D. E. Alvarez-Castillo, T. Fischer and S. Typel, Astron. Astrophys. **577**, A40 (2015).
 [7] X. H. Wu and H. Shen, Phys. Rev. C **96**, 025802 (2017).
 [8] R. C. Pereira, P. Costa, and C. Providência, Phys. Rev. D **94**, 094001 (2016).
 [9] P. Rehberg, S. P. Klevansky, and J. Hüfner, Phys. Rev. C **53**, 410 (1996).
 [10] H. Ueda, T. Z. Nakano, A. Ohnishi, M. Ruggieri, and K. Sumiyoshi, Phys. Rev. D **88**, 074006 (2013).
 [11] Peng-Cheng Chu, Bin Wang, Hong-Yang Ma, Yu-Min Dong, Su-Ling Chang, Chun-Hong Zheng, Jun-Ting Liu, and Xiao-Min Zhang, Phys. Rev. D **93**, 094032 (2016).
 [12] Y. Sugahara and H. Toki, Nucl. Phys. A **579**, 557 (1994).
 [13] S. S. Bao, J. N. Hu, Z. W. Zhang, and H. Shen, Phys. Rev. C **90**, 045802 (2014).
 [14] E. Annala, T. Gorda, A. Kurkela and A. Vuorinen, Phys. Rev. Lett. **120**, 172703 (2018).
 [15] B. P. Abbott *et al.* [LIGO Scientific and Virgo Collaborations], Phys. Rev. Lett. **119**, 161101 (2017).
 [16] C. Ishizuka, A. Ohnishi, K. Tsubakihara, K. Sumiyoshi and S. Yamada, J. Phys. G **35**, 085201 (2008).
 [17] I. Tews, J. M. Lattimer, A. Ohnishi, and E. E. Kolomeitsev, Astrophys. J. **848**, 105 (2017).
 [18] P. B. Demorest, T. Pennucci, S. M. Ranson, M. S. E. Roberts, and J. W. T. Hessels, Nature (London) **467**, 1081 (2010).
 [19] E. Fonseca *et al.*, Astrophys. J. **832**, 167 (2016).
 [20] J. Antoniadis *et al.*, Science **340**, 6131 (2013).
 [21] J. Nättilä, A. W. Steiner, J. J. E. Kajava, V. F. Suleimanov, and J. Poutanen, Astronomy & Astrophysics **591**, A25 (2016).
 [22] S. Guillot, and R. E. Rutledge, Astrophys. J. **796**, L3 (2014).
 [23] P. Haensel, M. Bejger, M. Fortin and L. Zdunik, Eur. Phys. J. A **52**, 59 (2016).